Enhancing the Optical Performance of Mid-Infrared Chalcogenide Glass Through Liquid Coating

Keke Chen[1,2], Xiange Wang[4], Yuyang Wang[1,2], Kai Jiao[1,2], Wei Tang[1,2], Xiang Shen[1,2], Shixun Dai[1,2], Qiuhua Nie[1,2], Rongping Wang[1,2], Pingxue Li[5], Vladimir Shiryaeve[6], and Xunsi Wang[1,2,3] * (iD)

[1] Laboratory of Infrared Materials and Devices, Advanced Technology Research Institute, Ningbo University, Ningbo 315211, China

[2] Zhejiang Key Laboratory of Photoelectric Materials and Devices, Ningbo 315211, China

[3] Ningbo Institute of Oceanography, Ningbo 315832, China

[4] College of Information and Intelligence Engineering, Zhejiang Wanli University, Ningbo 315000, China

[5] Faculty of Materials and Manufacturing, Beijing University of Technology, Beijing 100124, China

[6] Devyatykh Institute of Chemistry of High-Purity Substances of the Russian Academy of Sciences, 49 Tropinin Str., Nizhny Novgorod, 603951, Russia

*Correspondence: Xunsi Wang, wangxunsi@nbu.edu.cn

Abstract. Laser induced damage to optical component surfaces poses a critical challenge in the development of high-power laser systems. Such damage is typically influenced by its material host, defect distribution, laser parameters, and environmental conditions. The impact of surface defects becomes particularly pronounced under high-power, short-pulse laser irradiation, especially when surface roughness is suboptimal. In this study, we applied a liquid coating method to improve the surface quality of As_2S_3 glass under various surface conditions by eliminating defects with liquid. A detailed evaluation of the transmittance and surface laser damage threshold was conducted. The results reveal that effective liquid coating significantly reduces surface scattering and Fresnel reflection, resulting in up to a 24.8% increase in overall transmittance and a 2.17-fold improvement in the surface laser damage threshold. These findings underscore the critical role of liquid coating in enhancing optical material performance and offer a practical solution for optimizing high-power laser systems.

Keywords: Chalcogenide Glass, Surface Coating, Liquid Coating, Laser Damage

1. Introduction

Chalcogenide glasses are renowned for their exceptional optical properties, including wide transparent windows [1], high refractive indices, and relatively strong chemical stability [2]. These characteristics have enabled their applications across diverse fields such as fiber optics [3], infrared imaging [1], photonics [4], and environmental sensing [5]. However, during processing and usage, surface defects are prone to occur [6], leading to light scattering and thermal accumulation under high-power laser exposure. These issues significantly degrade the optical properties of chalcogenide glasses, such as transmittance and laser induced damage threshold (LIDT) [7]. Surface defects have thus become a critical factor limiting high energy laser transmission in these materials [8]. To address this, various surface treatment methods have been explored to reduce defects and improve optical performance. Traditional approaches include mechanical polishing [9], chemical polishing [10], laser polishing [11], an-

nealing [12], and coating [13]. Compared to traditional methods, coatings not only reduce surface defects but also provide protection for the glass surface during subsequent use [14]. Solid and liquid coatings have been widely studied for their ability to enhance optical properties. In 2014, A.B. Marouani deposited silica-based sol-gel coatings onto sandblasted glasses, achieving a transmission increase from 68.6% to 91.4%, nearly a 23% improvement [15]. However, the mismatch in the coefficient of thermal expansion (CTE) between solid coatings and the glass often leads to damage under high-power or extreme thermal conditions. In contrast, liquid coatings eliminate this issue, as the liquid facilitates stress relaxation and provides mobility to the system, thereby preventing such problems.

As early as 1975, P.E. Oettinger demonstrated a 25-fold improvement in the laser damage threshold of proustite crystals (75 MW/cm²) by applying a liquid arsenic-based coating [16]. In 1977, A.R. Chraplyvy and colleagues coated roughened NaCl and KBr surfaces with paraffin oil, achieving a nearly perfect optical surface due to the excellent refractive index matching between the liquid and alkali halides, effectively eliminating surface scattering caused by flaws or damage [17]. More recently, Zhao et al. developed a liquid-supply layer containing silicone oil droplets, which act as reservoirs for adaptive release. Under external stimulus, the liquid spreads over the surface, improving optical properties [18]. However, chalcogenide glass presents unique challenges due to its high thermal expansion coefficient and low softening point, making it difficult to find suitable solid or liquid coatings for mid-infrared applications [19]. While numerous reports detail solid coatings for chalcogenide glasses, such as antireflection (AR) coatings [20] and protective coatings [21]. The coating methods include physical vapor deposition (PVD) technology and magnetron sputtering technology, etc. [22]. In 2020, L.R. Robichaud et al. coated AsSe glass with Al_2O_3 AR-coating, and the single-sided coating increased the transmittance to 78%, which is 12.6% higher than that of uncoated [23]. Despite these advancements, liquid coatings for in-creasing the LIDT of chalcogenide glasses have yet to be investigated.

To address above challenge, we introduce a novel liquid coating method for mid-infrared chalcogenide glass, specifically As_2S_3, utilizing a compatible low *Tg* glass (*with a Tg lower than room temperature*) $As_{20}S_{60}I_{20}$ for surface coating. Initially, we performed various surface treatments on As_2S_3 to achieve different levels of surface roughness. Subsequently, the liquid coating was applied to As_2S_3 with varying roughness to eliminate surface defects, and the results were evaluated in terms of transmittance and surface LIDT. Additionally, an equivalent testing method was developed to correlate surface roughness with glass absorptivity, while the surface temperature distribution of As_2S_3 under laser irradiation was analyzed using the finite element method (FEM) and real time thermal monitoring. The findings reveal that liquid coating significantly reduces surface absorptivity in As_2S_3 samples, leading to an increase in overall transmittance by up to 24.8% and a 2.17-fold improvement in the surface laser damage threshold. These results underscore the critical role of liquid coating in enhancing the performance of mid-infrared chalcogenide glass and present a practical solution for optimizing high-power laser systems.

2. Experimental Procedures

2.1 Preparation of experimental samples

As_2S_3 glass was selected for testing due to its representative properties in the mid-infrared (MIR) range, including low light absorption in the 2 - 12 μm wavelength range, excellent chemical stability, and robust mechanical properties. The refractive index was measured using an infrared variable-angle spectroscopic ellipsometer (IR-VASE MARK II, J.A. Woollam Co.) and was determined to be 2.398 at 2.94 μm, as shown in Figure 1(a). The transmittance of the glass was analyzed using a Fourier-transform infrared spectrometer (Nicolet 380, USA) over the 2.5 - 13.5 μm wavelength range, as depicted in Figure 1(b). Within the 2.5 - 8 μm range, the transmittance was 68%, with no absorption peaks observed at 2.94 μm.
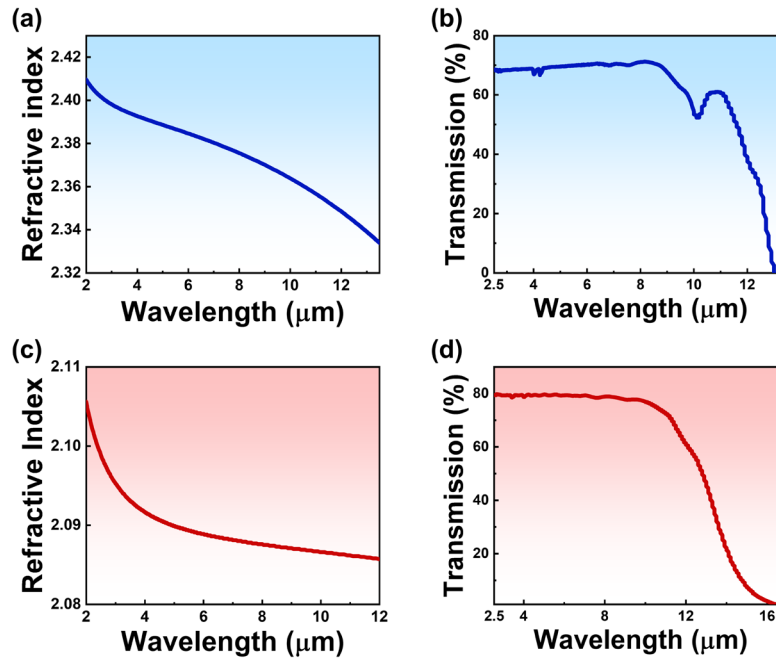
Figure 1. *The refractive index (a) and transmittance (b) of As_2S_3 (2mm); the refractive index (c) and transmittance (d) of $As_{20}S_{60}I_{20}$.*

Eight circular As_2S_3 glass samples (10 mm diameter, ~3 mm thickness) were prepared and labeled G1 - G8. Each sample was ground using sandpapers of varying particle sizes, as detailed in Table 1. Due to the use of Al_2O_3 polishing powder with a particle size of 20 nm, we consider a roughness of less than 20 nm to indicate a well-polished surface. Following this process, ultrasonic cleaning was performed to remove any dust, residual polishing powder, and glass debris from the surface.

Table 1. *Processing methods for each sample of G1-G8.*

Sample	Front surface of the glass	Back surface of the glass
G1、G5	13 μm ground	Well-Polished
G2、G6	6.5 μm ground	Well-Polished
G3、G7	3.4 μm ground	Well-Polished
G4、G8	Well-Polished	Well-Polished

2.2 Surface coating

$As_{20}S_{60}I_{20}$ (AsSI) glasses exhibit unique low-melting properties and represent the first example of inorganic glasses with high fluidity below 100°C [24]. In our experiment, the AsSI was used for liquid coating due to its liquid state at room temperature and low glass transition temperature (*Tg*) of 10.6°C. The viscosity of the glass is 0.98 Pa·s at 115 °C and greater than 1000 Pa·s at room temperature. As shown in Figure 1(c), it has a refractive index of 2.096 at 2.94 μm and a transmittance of 80% in the 2.5 - 10 μm wavelength range. To apply the coating, the As_2S_3 glass was placed flat on a table with its front side facing upward. AsSI was heated in a quartz syringe to 100℃ until fully liquefied, then carefully dropped onto the center of the samples G5 - G8 surface. A CaF_2 piece was used to cover and evenly spread the AsSI layer (the operational method is illustrated in Figure 2). Afterward, the sample was allowed to cool completely and use a vernier caliper to measure the coating thickness. After measurement, the coating thickness is ~0.08mm and it is uniform.
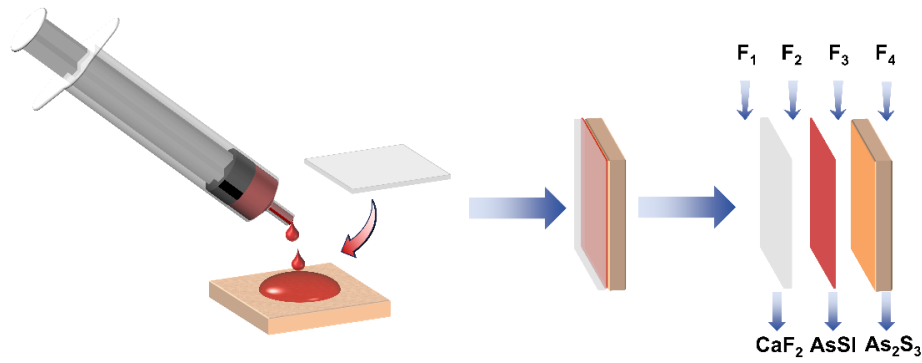
Figure 2. *Operation steps for AsSI coating method and CaF$_2$ covering method and the Fresnel reflection surface F1-F4.*

2.3 Roughness measurement

The surface roughness (R$_a$) along the sampling length were measured using a stylus pro-filometer (Model: DEKTAK 150). N refers to the number of valleys in the roughness generated curve after testing. Measurements were taken at three different locations on each sample. For liquid-coated samples (G5 - G8), measurements were conducted on the CaF$_2$ surface due to the coating coverage. A sampling length of 200 μm was used, and each measurement was repeated three times to obtain the mean values of roughness valley number. The reported data represent the averages of these measurements. The measurement precision of roughness was 0.01 μm, and the measurement precision of valleys was 1. Then the surface morphology was observed using a VHX-1000E microscope at 500x magnification, clearly revealing the surface features as shown in Figure 3.
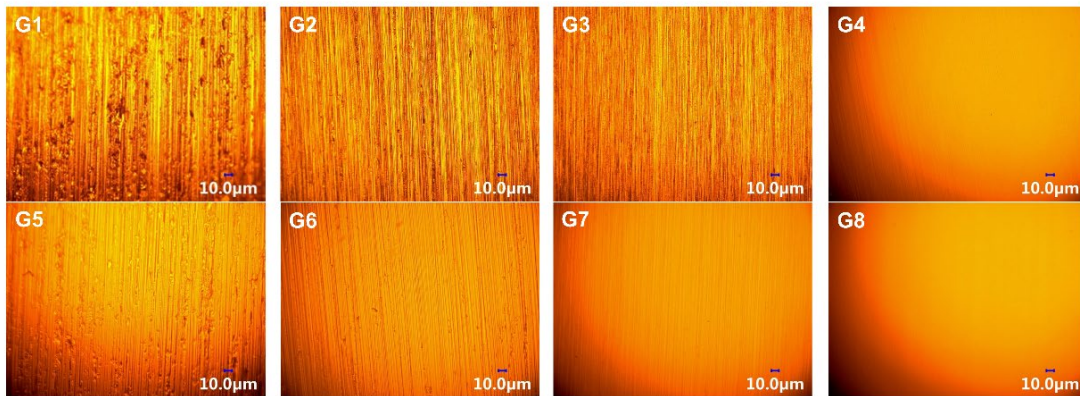

Figure 3. *Surface conditions observed As$_2$S$_3$ surface G1 - G4 and after liquid coating G5 - G8.*

The surface roughness and the valleys data for the control group (G1 - G4) and the liquid-coated group (G5 - G8) are presented in Table 2. The results show that as the treatment process becomes more refined, the surface roughness decreases. After AsSI coating and CaF$_2$ covering, the surface roughness of the glass was reduced to 2.46 μm. We also examined the surfaces of the control and liquid-coated groups under a microscope, as shown in Figure 3. When light was irradiated from the bottom of the glass, the microscope images clearly revealed that the surface of the control group (G1 - G4) remained rough, while the surface of the liquid-coated group (G5 - G8) became significantly smoother.

Table 2. Surface roughness test results for each sample of G1 - G8.

Sample	R_a (nm)	N
G1	453.88	174
G1	262.80	108
G2	50.10	93
G4	16.23	35
G5 - G8	2.46	30

2.4 Transmittance and LIDT measurement

The experiment is conducted at room temperature. The measurement setup is shown in Figure 4. The irradiation source was a long-pulse solid-state laser with a center wavelength of 2.94 μm, a pulse width of 0.5 ms, and a repetition frequency of 15 Hz. The transmittance measurement uses an unfocused laser with a spot size of 2mm, and tests with lower power to prevent laser damage to the surface. The sample was placed vertically in the optical path, and input and output power were recorded as transmittance data. LIDT measurement uses a CaF_2 lens with a focal length of 30 mm, resulting in a spot diameter of 500 μm. The sample was placed vertically in the optical path and the laser pulses were focused onto the front surface of As_2S_3. When measuring LIDT data, samples G1-G4 were served as control groups without surface coating, but similarly, CaF_2 was covered on their surfaces and fixed securely. The laser power was gradually increased, with a constant exposure time of 10 seconds maintained at each power level. To prevent thermal effects from accumulating, the laser was turned off for 5 minutes after each measurement. Measurements were repeated three times for each sample with varying roughness to enhance data reliability, and the re-ported data represent the averages of these measurements.
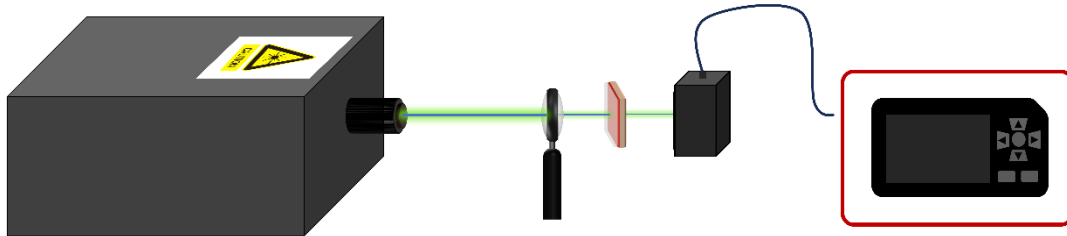
Figure 4. Optical setup for laser damage threshold measurement.

2.5 Temperature measurement

Capturing the temperature of glass at the exact moment of laser damage is challenging. To address this, a low-power continuous laser was used to irradiate the glass surface, and an infrared thermal imager was employed to measure the resulting temperature changes. The irradiation source was a solid-state laser with a center wavelength of 4.7 μm and a fixed incident energy of 2 W. The laser pulses were focused onto the front surface of the sample using a CaF_2 lens with a focal length of 30 mm, producing a spot diameter of 500 μm. The glass surface temperature was recorded using the infrared thermal imager over a 10-second exposure period. For reliability, each sample with varying surface roughness was measured three times at different positions, and the average values were calculated to minimize random errors.

3. Results and Discussions

3.1 Laser transmittance

For well-polished surfaces, Fresnel reflection at smooth interfaces with different refractive indices can lead to optical losses, particularly for chalcogenide glasses with high refractive indices. The refractive index of As2S3 chalcogenide glass is 2.398, that of AsSI is 2.096, the refractive index of CaF2 is 1.43, and that of air is 1. In the case of normal incidence, the Fresnel reflection is given by the formula:

$$r = \left(\frac{n_2 - n_1}{n_2 + n_1}\right)^2 \tag{1}$$

where n_1, n_2 are the refractive indices of the two media.

In this experiment, the optical elements have Fresnel reflection surfaces labeled F1 - F4 (as shown in Figure 2). F_1 is the Fresnel reflection between air and CaF_2, F_2 is the Fresnel reflection between CaF_2 and coating, F_3 is the Fresnel reflection between coating and As_2S_3, and F_4 is the Fresnel reflection between As_2S_3 and air. The total reflectance R can be calculated using the following formula:

$$R = 1 - (1 - F_1) * (1 - F_2) * (1 - F_3) * (1 - F_4) \tag{2}$$

The relationship between total reflectance and coating refractive index was calculated and shown in Figure 5(a). It can be seen that the largest reflectivity occurs when the gap is coated with air, and this reflectivity decreases from 35.3% to 22.2% as the refractive index of the coating medium increases from 1 to 1.848, and then slightly increases. Therefore, a material with a refractive index of 1.848 is the best as a coating medium. AsSI has a refractive index of 2.096, and this leads to a reflection of 22.8% as shown as a black dot in Figure 5(b), which is only a small difference from the optimal situation.
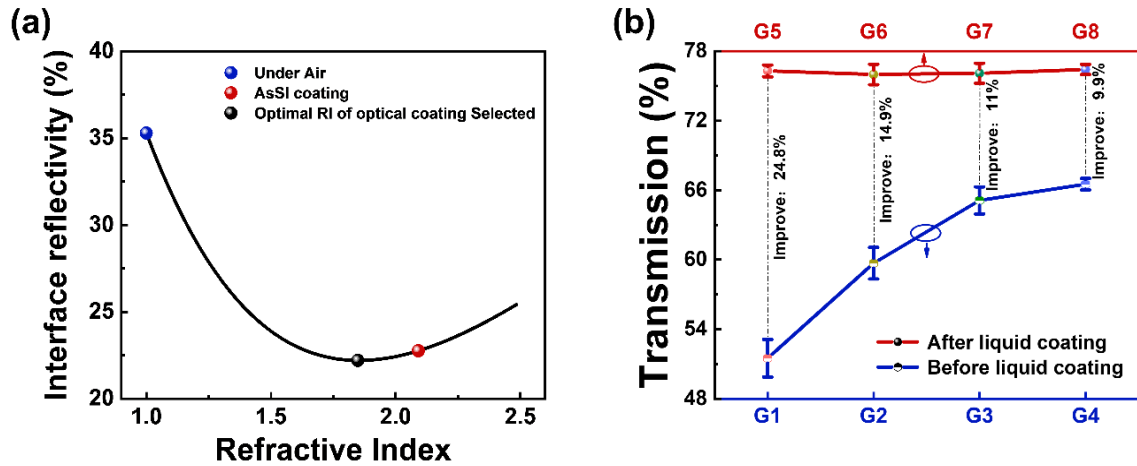

Figure 5. Theoretical calculation of Fresnel reflection (a); and transmission spectra of before and after liquid coating (b).

As shown in Figure 5(b), the transmittance of sample is only 51.5% for G1, increasing to 61.1% for G2, 65.1% for G3, and reaching 66.5% for G4. Finer grinding and polishing treatments effectively reduce surface defects and roughness. This is because the decrease in surface roughness also reduces light scattering, leadinging to an increase in transmittance [25]. After the liquid coating was applied, AsSI filled the rough surface, and as light passes through the filled interface, scattering is significantly reduced. Moreover, the refractive index of the

coating material is closer to As_2S_3 glass. This reduces the Fresnel reflection loss caused by refractive index mismatch, thereby improving the overall transmittance. So, the transmittance of samples G5 - G8 increased, reaching a maximum of 76%. The sum of the experimental transmission and calculated reflectivity (22.8% in Figure 5(a)) is 98.8%, with factors such as measurement errors accounting for the remaining loss. In addition, we also observed the interface area between the AsSI and As_2S_3 after coating as shown in Figure 6, and found that the interface quality was similar, which further proves that they can achieve similar transmittance after coating.
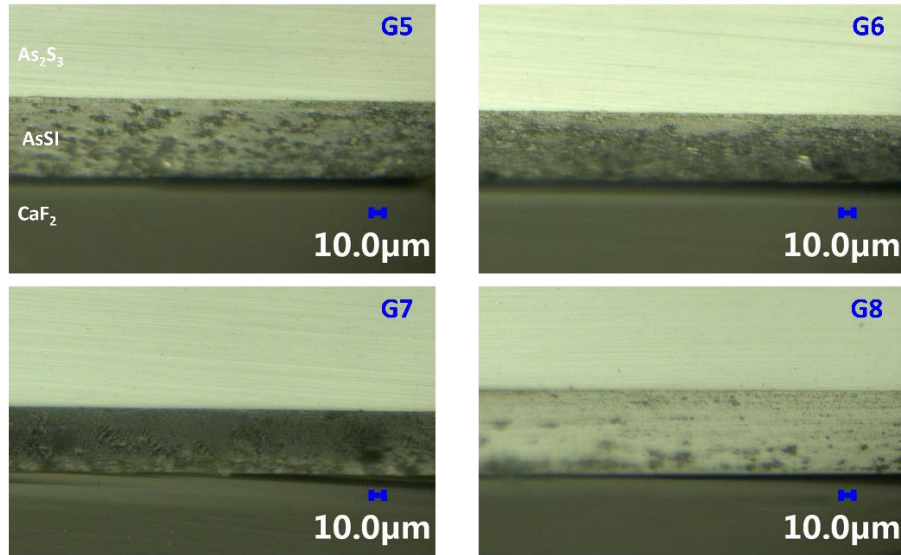

Figure 6. The interface area between the AsSI and As_2S_3 after coating (G5 - G8).

3.2 Laser damage

During the laser damage tests, damage was observed on the surfaces of both the control group and the liquid coating group. It should be noted that we have not observed any issues related to the coating flowing or detaching during the experimental process. Figure 7 illustrates the variations in the laser-induced damage threshold (LIDT) for both groups across different surface roughness levels. As the surface roughness decreases, the laser damage threshold increases progressively. These results indicate an inverse relationship between surface roughness and the laser damage threshold under pulsed laser irradiation. The laser damage threshold for sample G1 is only 92.7 J/cm², while sample G4 reaches 154.2 J/cm². Notably, the LIDT for the liquid-coated sample G5 peaks at 201.1 J/cm², which is 2.17 times greater than that of sample G1.
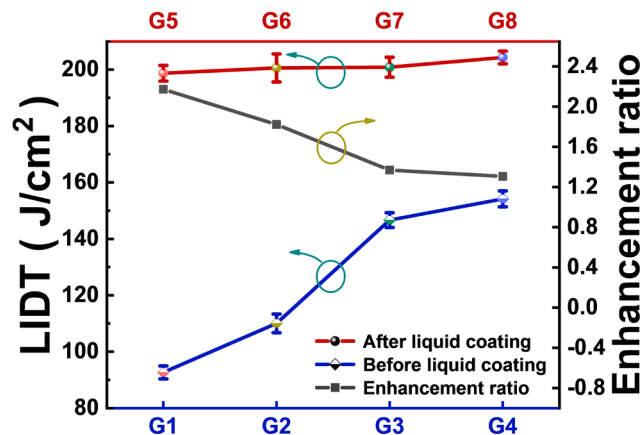

Figure 7. The LIDT before and after liquid coating of G1-G4 and the enhancement ratio of LIDT.

3.2.1 Surface temperature

Figure 8 shows the surface temperature of samples G1 - G8 under continuous irradiation with a 4.7 μm laser. For samples G1 - G4, the surface temperature increases with greater surface roughness, with the highest temperature of 86°C for G1 and 35.1°C for the polished sample G4. After liquid coating, the surface roughness decreases, resulting in a reduction in the surface temperature of samples G5 - G8 to between 30°C and 31°C.
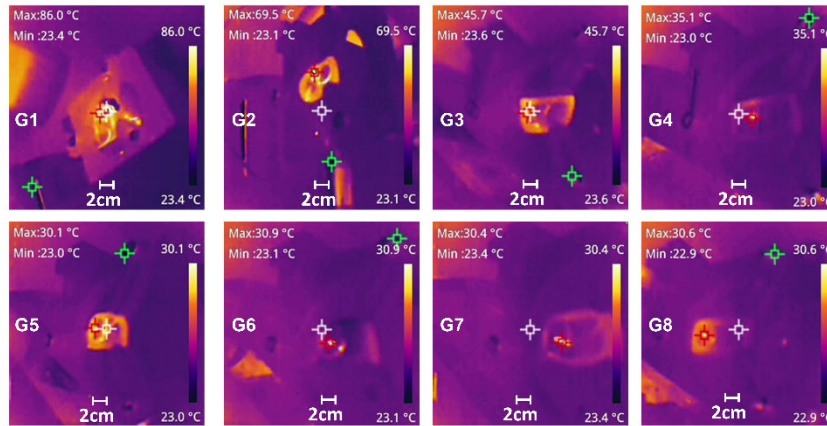

Figure 8. Surface temperature measured with infrared thermal imager of G1-G8.

3.2.2 Thermal damage theoretical model

Surface roughness is inherently complex, making it impractical to analyze every peak and valley in real applications. Therefore, we employ an equivalent treatment for rough surfaces [26]. For a given surface morphology, an inverted triangular folding model is applied, as illustrated in Figure 9.
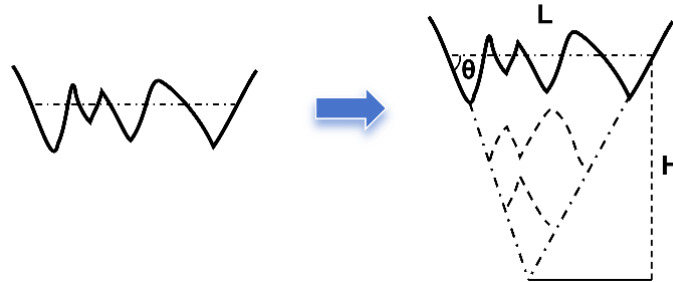

Figure 9. Treatment of rough surface with inverted triangle and downward folding.

The equivalent roughness inclination angle θ is defined as follows:

$$tan\,\theta = \frac{2H}{L} = \frac{8R_a N}{L} \tag{3}$$

L is the sampling length of 200 μm, and the value of N has been obtained during roughness measurement as shown in Table 2. Using this formula, the equivalent values of θ for different roughness profiles can be calculated out and shown in Table 3.

Table 3. The equivalent values of θ for different roughness profiles.

Sample	G1	G2	G3	G4	G5-G8
R_a (nm)	453.88	262.80	50.10	16.23	2.48
θ(°)	27.92	20.02	10.57	4.01	0.98

When a laser interacts with the material's surface, assuming no material absorption, just part of the light is reflected while the rest penetrates into the material. Let n_a and n_A represent the refractive indices of the incident and refractive media, respectively, where n_a=1 and n_A=2.398. Based on the Fresnel equation and the laws of refraction [27]:

$$cos\,\theta_t = \sqrt{1 - \left(\frac{n_a}{n_A} sin\,\theta_i\right)^2} \tag{4}$$

$$F = \frac{1}{2}\left(\left|\frac{n_a\,cos\,\theta_i - n_A\,cos\,\theta_t}{n_a\,cos\,\theta_i + n_A\,cos\,\theta_t}\right|^2 + \left|\frac{n_a\,cos\,\theta_t - n_A\,cos\,\theta_i}{n_a\,cos\,\theta_t + n_A\,cos\,\theta_i}\right|^2\right) \tag{5}$$

F is the reflectivity of As$_2$S$_3$ rough surface, θ_i is the incident angle (here, the value of θ_i is equal to θ) and θ_t is the transmission angle of the surface.

Then, the equivalent theoretical transmittance T_t can be calculated as:

$$T_t = (1 - F)^2 \tag{6}$$

The discrepancy between the calculated theoretical transmittance T_t and the measured transmittance shown in Figure 5 is attributed to the absorption of the glass sample. The absorptivity (A) for each sample is calculated and presented in Table 4.

Table 4. The absorptivity A for each sample of G1 - G8.

Sample	A (%)
G1	16.77
G1	9.92
G2	3.96
G4	1.96
G5-G8	1.46

From the absorption rate data of G5 - G8, the absorption coefficient α was calculated using Lambert law [28]:

$$A = 1 - e^{\alpha d} \tag{7}$$

Where α is the absorption coefficient and d is the samples' thickness. After calculation, α is 0.049 cm^{-1}, which is close to the absorption coefficient 0.03 cm^{-1} of As$_2$S$_3$ without OH$^-$ at 2.94 μm in [29].

To investigate the relationship between laser irradiation-induced surface temperature and roughness, a physical model was established to simulate the temperature field of chalcogenide glass under continuous laser irradiation. The model assumes vertical irradiation from a Gaussian-distributed laser beam with a waist beam radius of ω$_0$, and the simulation was con-ducted using COMSOL finite element software.

The sample has a radius of 0.5 cm and a thickness of 0.2 cm. Initially, the sample temperature is uniformly set to 298.15 K. Neglecting energy loss from thermal convection and radiation compared to laser energy, the back and side sur-faces of the sample are considered adiabatic for t > 0. The incident laser beam is modeled as axisymmetric and vertically irradiated onto the glass surface, assuming uniform and isotropic material properties under cylindrical coordinates. The heat distribution and variation on the glass surface are described using the heat conduction equation [30]:

$$\rho c \frac{\partial T}{\partial t} + \nabla(-k\nabla T) = Q \tag{8}$$

The material's density (ρ), specific heat capacity (c), and thermal conductivity (k) are considered, while Q denotes the volumetric heat source, representing the laser energy absorbed during interaction. The heat source, characterized as a Gaussian distribution [31], relates to the laser intensity (I_0) and absorption coefficient (A):

$$Q = AI_0 \tag{9}$$

Figure 10 illustrates the simulated and experimental surface temperatures of As$_2$S$_3$ glass under laser irradiation as a function of the equivalent roughness inclination angle θ. The results show that as the equivalent roughness angle increases, the surface temperature rises. After liquid coating (equivalent roughness angle θ = 0.98), the surface temperature is minimized. This is attributed to reduced roughness and absorptivity, leading to lower heat absorption. In contrast, higher roughness correlates with increased absorptivity and heat accumulation. The partial discrepancy between the experimental and simulation data arises from the idealized assumptions in the model, which simplifies the system's complexity. Factors such as material uniformity and laser irradiation consistency, which can influence the actual process, were not fully accounted for.
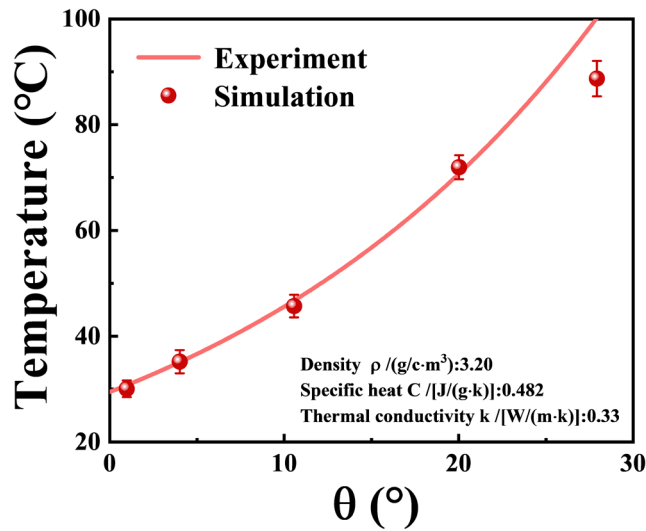

Figure 10. *Simulation and experiment of surface temperature of As$_2$S$_3$ glass with the equivalent roughness inclination angle θ under laser irradiation.*

4. Conclusion

In this study, we prepared As$_2$S$_3$ glass samples with varying surface roughness and applied liquid coatings to these surfaces. By establishing the relationship between surface roughness and laser absorptivity, we analyzed the impact of roughness on the optical properties of the glass. Our findings demonstrate that repairing surface defects on chalcogenide glass with an AsSI glass coating significantly enhances its optical performance, increasing transmittance by

24.8% and LIDT by 2.17 times. This research not only introduces a straightforward method for chalcogenide glass coating but also offers innovative insights and technical sup-port for the future development of high-performance, laser-resistant, mid-infrared optical mate-rials.

Data availability statement

The data supporting the findings of this study are available within the paper. Additional data are available from the corresponding author on reasonable request.

Author contributions

Conceptualization by Xunsi Wang, Keke Chen and Xiange Wang; Glass preparation and characterization by Wei Tang, Kai Jiao and Keke Chen; Data analysis and interpretation by Keke Chen and Yuyang Wang; Funding acquisition by Xunsi Wang; Writing, editing and review original draft by Keke Chen, Xiange Wang, Xunsi Wang, Xiang Shen, Shixun Dai, Qiuhua Nie, Rongping Wang, Pingxue Li and Vladimir Shiryaeve.

Competing interests

The authors declare that they have no competing interests.

Acknowledgement

References

[1] B. Bureau et al., "Recent advances in chalcogenide glasses", Journal of Non-Crystalline Solids, vol. 59, no. 21, pp. 276–283, Oct. 2004, doi: 10.1016/j.jnoncrysol.2004.08.096.

[2] A. Zakery and S. R. Elliott, "Optical properties and applications of chalcogenide glasses: a review", Journal of Non-Crystalline Solids, vol. 330, no. 1–3, pp. 1–12, Nov. 2003, doi: 10.1016/j.jnoncrysol.2003.08.064.

[3] D. Cai, Y. Xie, X. Guo, P. Wang, and L. Tong, "Chalcogenide Glass Microfibers for Mid-Infrared Optics", Photonics, vol. 8, no. 11, pp. 497-514, Nov. 2021, doi: 10.3390/photonics8110497.

[4] B. J. Eggleton, "Chalcogenide photonics: fabrication, devices and applications Introduction", Opt. Express, vol. 18, no. 25, pp. 26632-26634, Dec. 2010, doi: 10.1364/OE.18.026632.

[5] M.-L. Anne et al., "Chalcogenide Glass Optical Waveguides for Infrared Biosensing", Sensors, vol. 9, no. 9, pp. 7398–7411, Sep. 2009, doi: 10.3390/s90907398.

[6] T. Zhou, Z. Zhu, X. Liu, Z. Liang, and X. Wang, "A Review of the Precision Glass Molding of Chalcogenide Glass (ChG) for Infrared Optics", Micromachines, vol. 9, no. 7, pp. 337-357, Jul. 2018, doi: 10.3390/mi9070337.

[7] H. Truckenbrodt, A. Duparre, and U. Schuhmann, "Roughness and defect characterization of optical surfaces by light-scattering measurements", SPIE, Specification and Measurement of Optical Systems, vol.1971, pp.139-151, Jan. 1993, doi: 10.1117/12.141001.

[8] M. Zhan, Y. Zhao, G. Tian, H. He, J. Shao, and Z. Fan, "Stress, absorptance and laser-induced damage threshold properties of 355-nm HR coatings", Appl. Phys. B, vol. 80, no. 8, pp. 1007–1010, Jun. 2005, doi: 10.1007/s00340-005-1808-3.

[9] L. Wang, K. Zhang, Z. Song, and S. Feng, "Ceria concentration effect on chemical mechanical polishing of optical glass", Applied Surface Science, vol. 253, no. 11, pp. 4951–4954, Mar. 2007, doi: 10.1016/j.apsusc.2006.10.074.

[10] C. Iliescu, B. Chen, and J. Miao, "On the wet etching of Pyrex glass", Sensors and Actuators A, vol. 143, no.1, pp. 154-161, Nov. 2007, doi: 10.1016/j.sna.2007.11.022.

[11] A. Krishnan and F. Fang, "Review on mechanism and process of surface polishing using lasers", Front. Mech. Eng., vol. 14, no. 3, pp. 299–319, Sep. 2019, doi: 10.1007/s11465-019-0535-0.

[12] T. Zhou, Q. Zhou, J. Xie, X. Liu, X. Wang, and H. Ruan, "Surface defect analysis on formed chalcogenide glass $Ge_{22}Se_{58}As_{20}$ lenses after the molding process", Appl. Opt., vol. 56, no. 30, pp. 8394-8402, Oct. 2017, doi: 10.1364/AO.56.008394.

[13] H. A. Macleod, "Recent developments in deposition techniques for optical thin films and coatings", in Optical Thin Films and Coatings, Elsevier, pp. 3–23. 2018, doi: 10.1016/B978-0-08-102073-9.00001-1.

[14] G. Womack, K. Isbilir, F. Lisco, G. Durand, A. Taylor, and J. M. Walls, "The performance and durability of single-layer sol-gel anti-reflection coatings applied to solar module cover glass", Surface and Coatings Technology, vol. 358, pp. 76–83, Jan. 2019, doi: 10.1016/j.surfcoat.2018.11.030.

[15] A. Marouani, N. Bouaouadja, Y. Castro, and A. Durán, "Repair and Restoration of the Optical Properties of Sandblasted Glasses By Silica-Based Sol-Gel Coatings", Int J of Appl Glass Sci, vol. 6, no. 1, pp. 94–102, Mar. 2015, doi: 10.1111/ijag.12088.

[16] P. E. Oettinger, "Liquid coatings to decrease laser-induced surface damage in proustite", Optics Communications, vol. 13, no. 4, pp. 431–434, Apr. 1975, doi: 10.1016/0030-4018(75)90139-X.

[17] A. R. Chraplyvy, "Liquid surface coating for optical components used in high power laser applications", Appl. Opt., vol. 16, no. 9, pp. 2491–2494, Sep. 1977, doi: 10.1364/AO.16.002491.

[18] H. Zhao, L. O. Prieto-López, X. Zhou, X. Deng, and J. Cui, "Multistimuli Responsive Liquid-Release in Dynamic Polymer Coatings for Controlling Surface Slipperiness and Optical Performance", Adv Materials Inter, vol. 6, no. 20, p. 1901028, Oct. 2019, doi: 10.1002/admi.201901028.

[19] Liu Zhuo, Yang Xiaojing, Xie Qiming, Yang Weisheng, and Wang Xueying, "Research Progress of Infrared Optical Thin Filmson Chalcogenide Glass Substrates", Laser Optoelectron. vol. 59, no. 21, p. 2100003, Nov. 2022, doi: 10.3788/LOP202259.2100003.

[20] K. M. Khajurivala, "Erosion resistant anti-reflection coating for ZnSe, CZnS, chalcogenide, and glass substrates", SPIE Defense, Security, and Sensing, vol. 8012, p.801242, May 2011, p. 801242. doi: 10.1117/12.896905.

[21] J. H. Lee, H. Kim, W. H. Lee, M. C. Kwon, and Y. G. Choi, "Surface modification of chalcogenide glass for diamond-like-carbon coating", Applied Surface Science, vol. 478, pp. 802–805, Jun. 2019, doi: 10.1016/j.apsusc.2019.02.043.

[22] C.-S. Park et al. "Effect of boron and silicon doping on the surface and electrical properties of diamond like carbon films by magnetron sputtering technique", Surface & Coatings Technology, vol.213, pp. 131–134, Sep. 2013, doi: 10.1016/j.surfcoat.2012.01.014.

[23] L.R. Robichaud et al., "High-power supercontinuum generation in the mid-infrared pumped by a soliton self-frequency shifted source", Optics Express, vol.28, no. 1, pp. 107–115, Jan. 2020, doi: https://doi.org/10.1364/OE.380737.

[24] S. S. Flaschen, A. D. Pearson, and W. R. Northover, "Low Melting Sulfide-Halogen Inorganic Glasses", Journal of Applied Physics, vol. 31, no. 1, pp. 219–220, Jan. 1960, doi: 10.1063/1.1735409.

[25] J. C. Stover, M. L. Bernt, and E. L. Church, "Measurement and analysis of scatter from rough surfaces", Stray Radiation in Optical Systems III, vol. 2260, pp. 40–49, Oct. 1994, doi: https://doi.org/10.1117/12.189225.

[26] Hongze Wang et al., "A model to calculate the laser absorption property of actual surface", International Journal of Heat and Mass Transfer, vol. 118, pp. 562–569, Mar, 2018, doi: 10.1016/j.ijheatmasstransfer.2017.11.023.

[27] A. I. Lvovsky, "Fresnel Equations", Encyclopedia of Optical and Photonic Engineering (Print) - Five Volume Set, 2nd ed., Boca Raton: CRC Press, 2015, pp. 838–843. doi: 10.1081/E-EOE2-120047133.

[28] J. Müllerová et al., "Optical Absorption in Si:H Thin Films: Revisiting the Role of the Refractive Index and the Absorption Coefficient", Coatings, vol. 11, no. 1081, pp.1–10, Sep, 2021, doi: 10.3390/coatings11091081.

[29] Y. Wang et al., "Impacts of hydroxyl and bond energy on laser-induced damage in mid-infrared chalcogenide glass.", J Am Ceram Soc., vol. 274, no. 1-2, pp.100–105, Nov, 2024, doi: 10.1111/jace.20256.

[30] M. N. Ozisik, "A Heat/Mass Analogy for Fission-Product Deposition from Gas Streams", Nuclear Science and Engineering, vol. e20256, pp. 1 - 8, Jun. 1964, doi: 10.13182/NSE64-A28905.

[31] S. Papernov and A. W. Schmid, "Laser-induced surface damage of optical materials: absorption sources, initiation, growth, and mitigation", Laser-induced Damage in optical Materials. vol. 7132, pp. 7132J-1-28. 2008, doi: 10.1117/12.804499.